


Article

Pressure-Driven Nitrogen Flow in Divergent Microchannels with Isothermal Walls

Amin Ebrahimi ^{1,*}, Vahid Shahabi ² and Ehsan Roohi ³

¹ Department of Materials Science and Engineering, Delft University of Technology, Mekelweg 2, 2628 CD Delft, The Netherlands

² Department of Mechanical Engineering, Faculty of Engineering, Ferdowsi University of Mashhad, Mashhad, Khorasan Razavi P.O. Box 91775-1111, Iran; v.shahabi69@gmail.com

³ State Key Laboratory for Strength and Vibration of Mechanical Structures, International Center for Applied Mechanics, School of Aerospace Engineering, Xi'an Jiaotong University, Xianning West Road, Beilin District, Xi'an 710049, China; e.roohi@xjtu.edu.cn

* Correspondence: A.Ebrahimi@tudelft.nl

Abstract: Gas flow and heat transfer in confined geometries at micro- and nanoscales differ considerably from those at macro-scales, mainly due to nonequilibrium effects such as velocity slip and temperature jump. Nonequilibrium effects increase with a decrease in the characteristic length-scale of the fluid flow or the gas density, leading to the failure of the standard Navier–Stokes–Fourier (NSF) equations in predicting thermal and fluid flow fields. The direct simulation Monte Carlo (DSMC) method is employed in the present work to investigate pressure-driven nitrogen flow in divergent microchannels with various divergence angles and isothermal walls. The thermal fields obtained from numerical simulations are analysed for different inlet-to-outlet pressure ratios ($1.5 \leq \Pi \leq 2.5$), tangential momentum accommodation coefficients, and Knudsen numbers ($0.05 \leq Kn \leq 12.5$), covering slip to free-molecular rarefaction regimes. The thermal field in the microchannel is predicted, heat-lines are visualised, and the physics of heat transfer in the microchannel is discussed. Due to the rarefaction effects, the direction of heat flow is largely opposite to that of the mass flow. However, the interplay between thermal and pressure gradients, which are affected by geometrical configurations of the microchannel and the applied boundary conditions, determines the net heat flow direction. Additionally, the occurrence of thermal separation and cold-to-hot heat transfer (also known as anti-Fourier heat transfer) in divergent microchannels is explained.

Keywords: Poiseuille micro-flow; thermal field analysis; heat flow; divergent microchannel; direct simulation Monte Carlo (DSMC)



Citation: Ebrahimi, A.; Shahabi, V.; Roohi, E. Pressure-Driven Nitrogen Flow in Divergent Microchannels with Isothermal Walls. *Appl. Sci.* **2021**, *11*, 3602. <https://doi.org/10.3390/app11083602>

Communicated by: Mehdi Jangi

Received: 15 March 2021

Accepted: 14 April 2021

Published: 16 April 2021

Publisher's Note: MDPI stays neutral with regard to jurisdictional claims in published maps and institutional affiliations.



Copyright: © 2021 by the authors. Licensee MDPI, Basel, Switzerland. This article is an open access article distributed under the terms and conditions of the Creative Commons Attribution (CC BY) license (<https://creativecommons.org/licenses/by/4.0/>).

1. Introduction

Gas flow in micro- and nano-channels with nonuniform cross-sections offers opportunities to develop small devices with novel applications (see, for example, [1–6]). Understanding heat and fluid flow in microchannels is essential to engineer novel micro-electromechanical systems (MEMS) [7–9]. However, this is a challenging task since the rate of collisions between the gas molecules and solid walls reduces with decreasing characteristic length-scale of the fluid flow or the gas density, affecting the random movement of molecules, which is commonly known as nonequilibrium effects [10,11]. Nonequilibrium molecular transport processes cause velocity slip and temperature jump at walls, and influence thermal and fluid flow fields [12,13]. The Knudsen number (Kn), which is the ratio of the molecular mean free path λ to a characteristic length scale \mathcal{L} , is often employed as an indicator of deviation from the equilibrium condition. The higher the Knudsen number, the higher the deviation from the equilibrium condition. Four different rarefaction regimes have been defined based on the Knudsen number [14], and are commonly named the free molecular ($Kn > 10$), transition ($10^{-1} \leq Kn \leq 10$), slip ($10^{-3} \leq Kn \leq 10^{-1}$), and continuum ($Kn \leq 10^{-3}$) regimes.

Micro-devices usually operate in the slip and transition rarefaction regimes at standard pressure and temperature [12]. It is widely acknowledged that the standard Navier–Stokes–Fourier (NSF) equations fail to accurately predict thermal and fluid flow fields when the nonequilibrium effects are significant [15–17]. The Boltzmann equation governs fluid flow at micro-scales in the entire range of Knudsen numbers [18]. However, the direct numerical solution of the Boltzmann equation is generally expensive with available computational capabilities, and is limited to simple applications because of the high dimensionality of the Boltzmann equation and the complexity of the collision integral. Moreover, the application of the Boltzmann equation is limited to dilute gasses due to the assumption of binary intermolecular collisions [19]. The direct simulation Monte Carlo (DSMC) method is a numerical technique that has been developed based on the kinetic theory to approximate the solution of the Boltzmann equation [18].

Zheng et al. [20] compared the numerical predictions obtained from DSMC simulations with the solutions of the NSF equations for a Poiseuille gas flow between two parallel plates, and reported quantitative and qualitative differences between the predictions. Deviations between numerical predictions obtained using the DSMC method and the NSF equations increases with increasing Knudsen number [20–23]. Using the regularised 13-moment equations, Torrilhon and Struchtrup [24] achieved better agreement with the DSMC results up to $Kn \approx 1$ in comparison with the NSF-based solutions. Varoutis et al. [25] studied Poiseuille gas flow in channels with finite lengths using the DSMC method, and reported that the nonequilibrium effects are the most significant factor affecting rarefied gas flow in channels.

The majority of the published literature on subsonic internal gas flows at micro-scales is limited primarily to flow passages with uniform cross-sections [26–28]. Moreover, previous studies mostly focused on characterising pressure loss, mass flow rate, and velocity field [29]. There is a crucial lack of detailed thermal field analyses of gas flow in micro- and nanochannels with nonuniform cross-sections in which nonequilibrium effects play an important role [30]. Using the NSF equations with the first-order slip boundary condition, Varade et al. calculated temperature variations in divergent [31] and convergent [32] microchannels for both continuum and slip flow regimes. Using the same approach, Hemadri et al. [33,34] calculated temperature distribution in convergent microchannels in the slip and early-transition rarefaction regimes. Milićević and Stevanović [35] proposed an analytical solution to the one-dimensional NSF equations to describe steady-state pressure-driven isothermal gas flow in microchannels with variable cross-sections. Ohwada et al. [36] stated that heat and mass flow are in opposite directions for Poiseuille flow between two parallel plates for $Kn > 10^{-1}$, whereas they are in the same direction adjacent to the walls at low Knudsen numbers. Notably, only the tangential heat flow profiles were considered in their study, but both normal and tangential heat fluxes contribute to the net heat flow. John et al. [37] numerically studied the influence of the pressure ratio and surface accommodation coefficient on the thermal field of a Poiseuille gas flow between two parallel plates. The DSMC method has recently been employed to investigate temperature variations in divergent microchannels [38–40]. Characterising the thermal field in microchannels with nonuniform cross-sections is emerging for micro- and nano-system engineering, so further investigations are essential.

Despite the extensive interest in studying fluid flow at the micro- and nanoscales, numerical investigations of gas flow under nonequilibrium conditions are deficient in thermal analyses. Previous studies on thermal field analysis in microfluidics systems are mostly limited to the channels with uniform cross-sections (see, for instance, [37,41–48]). Therefore, there is an indispensable need for detailed investigations on heat and fluid flow at the micro- and nanoscales under nonequilibrium conditions. The goal of the present study was to enhance our understanding of heat and fluid flow in divergent microchannels, which are applicable in micro-devices such as micro-pumps, micro-actuators, and micro-thrusters. Numerical simulations based on the DSMC method were performed to explore the effects of divergence angle, inlet-to-outlet pressure ratio, rarefaction, and tangential

momentum accommodation coefficient on thermal and fluid flow fields. Heat and fluid flows under nonequilibrium conditions are considerably different from their equilibrium counterpart, providing the motivation to conduct the present study.

2. Problem Description

A probabilistic numerical approach based on the direct simulation Monte Carlo method was employed to study steady-state, pressure-driven, Poiseuille gaseous nitrogen flow in divergent microchannels shown schematically in Figure 1. The divergence angle of the channel (ϕ) is defined as follows [39]:

$$\phi = \frac{100 \cdot (H_o - H_i)}{L}, \quad (1)$$

where H_i and H_o are the height of the channel at the inlet and the outlet, respectively. The length of the channel (L) is twenty times larger than its inlet height (i.e., $L = 20 \times H_i = 8 \times 10^{-6}$ m). The problem is assumed to be two-dimensional, which is a valid assumption for channels with considerably large depths [43,49]. The molecular properties of gaseous nitrogen are summarised in Table 1, where d_p is molecular diameter, m_p is molecular mass, ω is the viscosity-temperature index, T_{ref} is the reference temperature in the viscosity-temperature relation, and μ_0 is the viscosity at the reference temperature.

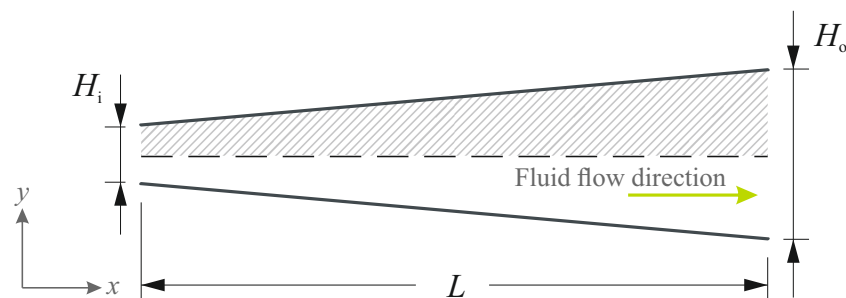


Figure 1. Schematic of the divergent microchannel considered in the present study. The hatched region was considered for calculations.

Due to the symmetric configuration of the channel and the flow field, one-half of the physical domain (the hatched region in Figure 1) was considered for calculations. Heat and fluid flow in the channel are described in a Cartesian coordinate system. The temperature of the solid walls (T_w) and the gas at the inlet (T_i) is constant, equal to 300 K. The Knudsen number is defined based on the inlet height, i.e., $Kn = \lambda/H_i$. The inlet-to-outlet pressure ratio (Π) is defined as p_i/p_o and the gas pressure at the channel inlet (p_i) is calculated based on the Knudsen number and the ideal gas law. The effects of tangential momentum accommodation coefficient (α) on thermal and fluid flow fields were also studied in the present work. The tangential momentum accommodation coefficient ranges between zero (specular reflection) and one (fully-diffused reflections) depending on the internal gas molecule structure, the molecular mass of the gas, and the surface material [50,51].

Table 1. Molecular properties of gaseous nitrogen.

d_p (m)	m_p (kg)	DOF_{rot} (–)	ω (–)	T_{ref} (K)	μ_0 (N s m ^{−2})
4.17×10^{-10}	4.65×10^{-26}	2	7.4×10^{-1}	300	1.656×10^{-5}

3. Numerical Procedure

An extended version of the dsmcFoam solver [52], which was developed within the framework of an open-source solver (OpenFOAM), was employed in the present study. This solver

has been meticulously validated for a variety of benchmark cases [52–54] including sub-sonic Poiseuille micro-flows. The variable hard sphere (VHS) model was selected to treat the binary intermolecular collisions. The energy exchange between both translational and rotational modes was allowed. The no-time-counter (NTC) [18] collision sampling model was chosen. Additionally, the transient adaptive sub-celling (TAS) scheme [55] was utilised to divide collision cells every time-step according to the number of particles inside each collision cell, to have at least two simulator particles in each subcell. This resulted in the selection of collision partners that are located within a relative distance smaller than the local molecular mean free path.

Oran et al. [56] suggested a cell size of $\lambda/3$ to capture the gradients in flow fields. In the case of low-speed micro-flows, larger grids might be employed in the stream-wise direction due to insignificant flow gradients [57–60]. After a grid independence test, a grid with cell sizes of $\lambda/4$ and $\lambda/2$ in the normal and the stream-wise directions, respectively, was selected. To capture the flow gradients for the cases with $\text{Kn} > 2.5 \times 10^{-1}$, the grid size was the same as that for the cases with $\text{Kn} = 2.5 \times 10^{-1}$. All simulations were initialised with 50 particles per cell to minimise statistical relations between particles [61] and to have at least 15 particles in the computational cells adjacent to the channel's outlet. The time-step was selected to be sufficiently smaller than the local mean collision time so particles stayed inside a cell for multiple time-steps. To return the relevant macroscopic data, the results were sampled over 3×10^6 time-steps after achieving the steady-state condition. The sample size was sufficiently large to let the solution procedure continue even after equating the inlet and outlet mass flow rates, leading to a converged solution with negligible (less than 1%) statistical noise [62–64]. Each simulation was carried out in parallel on four cores of an Intel Core i7-3520M processor, and required roughly 200 h to complete.

4. Model Validation and Verification

The Poiseuille argon flow in a microchannel with a uniform cross-section was considered to verify the reliability of the present model. The microchannel length was $15 \mu\text{m}$ and its height was $1 \mu\text{m}$. Gaseous argon entered the channel with a constant temperature of 300 K, and the inlet-to-outlet pressure ratio Π was set to 3. The channel walls were assumed to be fully diffuse (i.e., $\alpha = 1$), and their temperature was set to 300 K. Four different cases with different Knudsen numbers were studied, which cover the slip and transition rarefaction regimes. For each case, about 1.5×10^6 DSMC simulator particles were utilised. The predicted pressure and Mach number (Ma) distributions along the microchannel centreline are shown in Figure 2. The Mach number is defined as follows:

$$\text{Ma} = \frac{\|\vec{V}\|}{\sqrt{\gamma RT}}, \quad (2)$$

where \vec{V} is the fluid velocity vector, γ is the ratio of specific heat of nitrogen at a constant pressure to its specific heat at a constant volume, R is the specific gas constant, and T is the temperature. The results are in reasonable agreement with the data reported by White et al. [64]. Further comparison of the results obtained from the present model with experimental, analytical, and numerical data was performed for gaseous nitrogen flow in divergent microchannels, and can be found in [31,38,39].

Figure 3 shows the influence of grid size, number of simulator particles per cell (PPC), and time-step size on the results obtained from the present DSMC simulations. For this study, nitrogen flow in a microchannel with uniform cross-section ($\phi = 1$), $\text{Kn}_i = 0.1$ (transition rarefaction regime), and the inlet-to-outlet pressure ratio Π of 2.5 was considered.

To determine an appropriate time-step size Δt within which the molecular movement and collision are distinguishable, the following correlations were employed:

$$\Delta t_c = \frac{0.2\lambda}{\sqrt{\frac{2\kappa_b T}{m_p}}}, \tag{3}$$

$$\Delta t_t = \frac{0.5\Delta x}{\sqrt{\frac{2\kappa_b T}{m_p}}}, \tag{4}$$

where Δt_c is the mean collision time, Δt_t is the mean transit time, and κ_b is the Boltzmann constant. The time-step size Δt was defined as a fraction of the minimum value of Δt_c and Δt_t (i.e., $\Delta t = \zeta \cdot \min(\Delta t_c, \Delta t_t)$ and $\zeta \leq 1$). For the range of parameters studied in the present work, the results are practically insensitive to the grid size, number of simulator particles per cell, and time-step size.

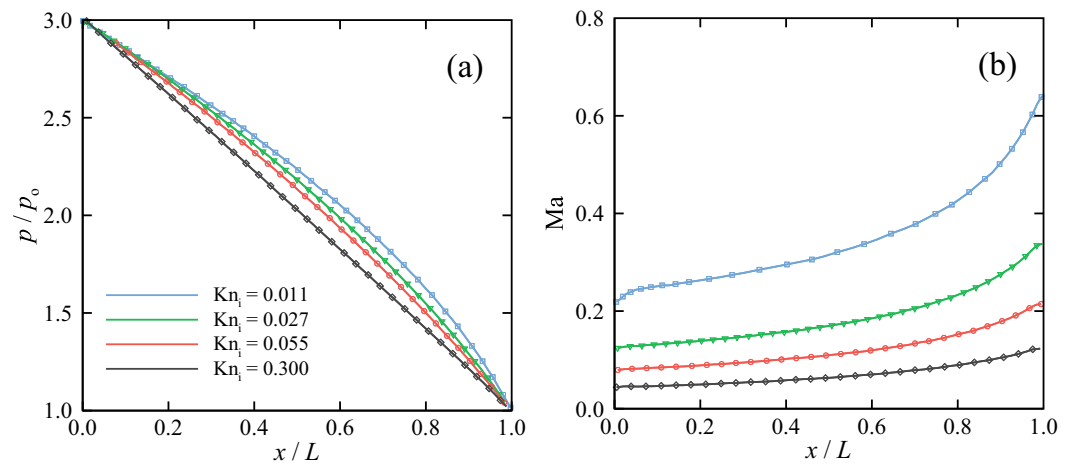


Figure 2. Comparison of the numerical results obtained from the present model (solid lines) with the data reported by White et al. [64] (symbols) for pressure-driven rarefied argon flow in a microchannel with a uniform cross-section. Profiles of (a) pressure and (b) Mach number along the microchannel centreline.

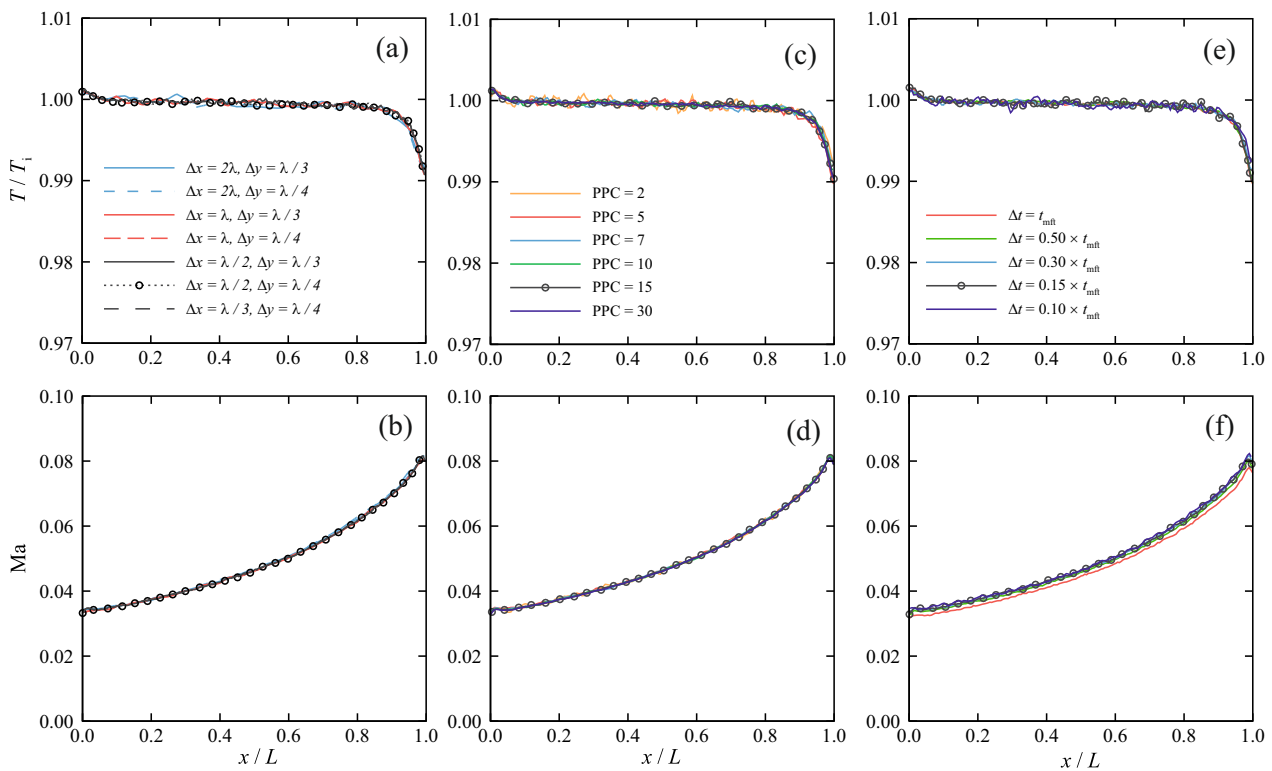


Figure 3. The effects of (a,b) the computational grid size, (c,d) number of simulator particles per cell, and (e,f) time-step size on the predicted profiles of temperature and Mach number along the channel centreline. $Kn_i = 0.1$, $\phi = 1$ and $\Pi = 2.5$. Curves shown with symbols indicate the chosen values.

5. Results and Discussion

The influence of the microchannel divergence angle on variations in temperature and Mach number along the microchannel centreline is shown in Figure 4. For $\phi < 2.5$, the gas temperature decreases along the channel because of the augmentation of the gas velocity toward the channel outlet. The increase in kinetic energy of the gas results in a reduction in its internal energy and thus its temperature. The gas velocity remains almost constant along the channel with $\phi = 2.5$, and the gas temperature hardly changes along the channel, except in regions close to the inlet and outlet boundaries. Further increase in the divergence angle ϕ results in a decrease in gas velocity along the channel, which is attributed to the increased cross-sectional area of the channel as well as the increased shear stress at the channel walls [31,39]. The kinetic energy of the gas converts into internal energy as the fluid velocity decreases toward the channel outlet for the cases with $\phi > 2.5$, leading to an increase in gas temperature. Additionally, the bulk gas temperature reduces with an increase in divergence angle of the channel because of the increased bulk gas velocity and the reduced rate of molecular collision. Because of the development of a viscous boundary layer close to the channel inlet [39,64], the gas flow accelerates in the entrance region; however, the flow decelerates after passing this region moving toward the channel outlet to conform to the pressure prescribed at the outlet. Close to the channel outlet ($x/L > 0.9$), the gas temperature drops, which is attributed to the rapid gas expansion in that region, which is known as the expansion cooling phenomenon [20,65]. A similar behaviour close to the channel outlet has been reported by others [28,37,43–45] for Poiseuille micro-flows in microchannels with uniform cross-sections.

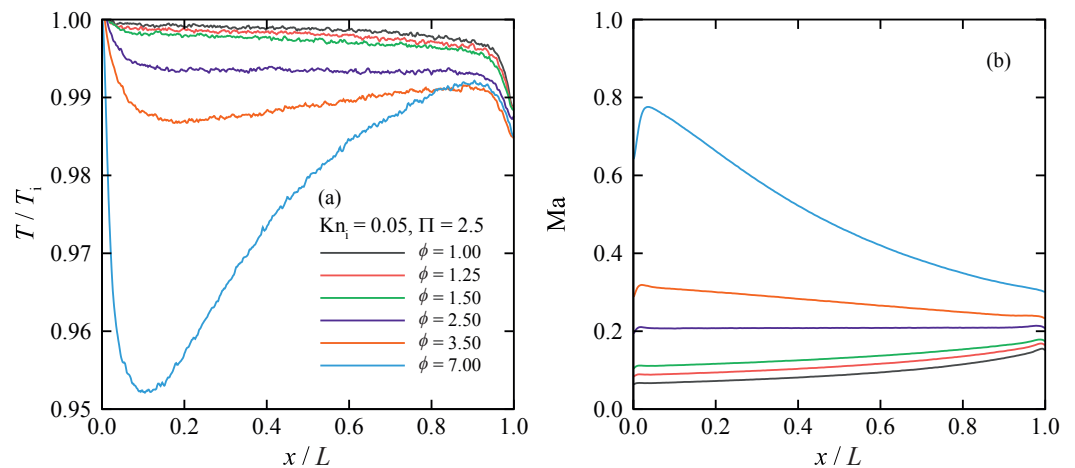


Figure 4. Distribution of (a) gas temperature and (b) Mach number along the microchannel centreline for different divergence angles ϕ ($Kn_i = 0.05$ and $\Pi = 2.5$). The inlet temperature (T_i) is used to non-dimensionalise the predicted temperatures.

The overall heat flow direction for the problem considered in the present work is determined by both the thermal and pressure gradients in the microchannel [66]. The heat flow direction and contours of dimensionless temperature (T/T_i) obtained from the DSMC simulations are shown in Figure 5 for microchannels with different divergence angles at $Kn_i = 0.05$ and $\Pi = 2.5$. Heat flows generally toward the channel inlet, except in regions adjacent to the walls in the Knudsen layer, where the heat flow is dominated by viscous heating. For the cases with $\phi > 2.5$, the amount of heat induced by viscous dissipation decreases along the microchannel due to the reductions in wall shear stress and slip velocity [39], decreasing the influence of viscous dissipation on the net heat flow direction in regions close to the walls. In contrast, the amount of heat generated by viscous dissipation increases as the gas moves along the channels with $\phi \leq 2.5$, increasing its influence on the net heat flow direction in regions adjacent to the walls. Accordingly, it can be argued that the heat flow is dominated by the pressure gradient (known as a rarefaction effect [66]) in microchannels with a divergence angle of $\phi \leq 2.5$. Due to the rarefaction effects, heat flow from cold to hot regions is observed, which is not predictable using the NSF equations because of the neglect of high-order rarefaction terms [67]. Heat flow in the central region of the channel is dominated by the mass flow driven by the pressure gradient. However, the magnitude of the thermal gradient increases with an increase in divergence angle ϕ , affecting the net heat flow direction. For cases with $\phi > 2.5$, a thermal separation occurs at a certain location in the channel beyond which heat flows toward the channel outlet. Thermal separation for pressure-driven gas flow in microchannels of variable cross-sections is attributed to the enhanced contribution of thermal gradient to the total heat transfer [68]. The position of the thermal separation point moves toward the inlet with an increase in the divergence angle of the channel. Notably, no hydrodynamic separation was observed for the cases considered in the present study [38,39]. These observations can also be explained through the asymptotic analysis of the Boltzmann equation [66] for small Knudsen numbers (i.e., slip and early-transition regimes). However, this type of analysis, which is based on the continuum theory, fails to accurately predict heat transfer at high Knudsen numbers [38].

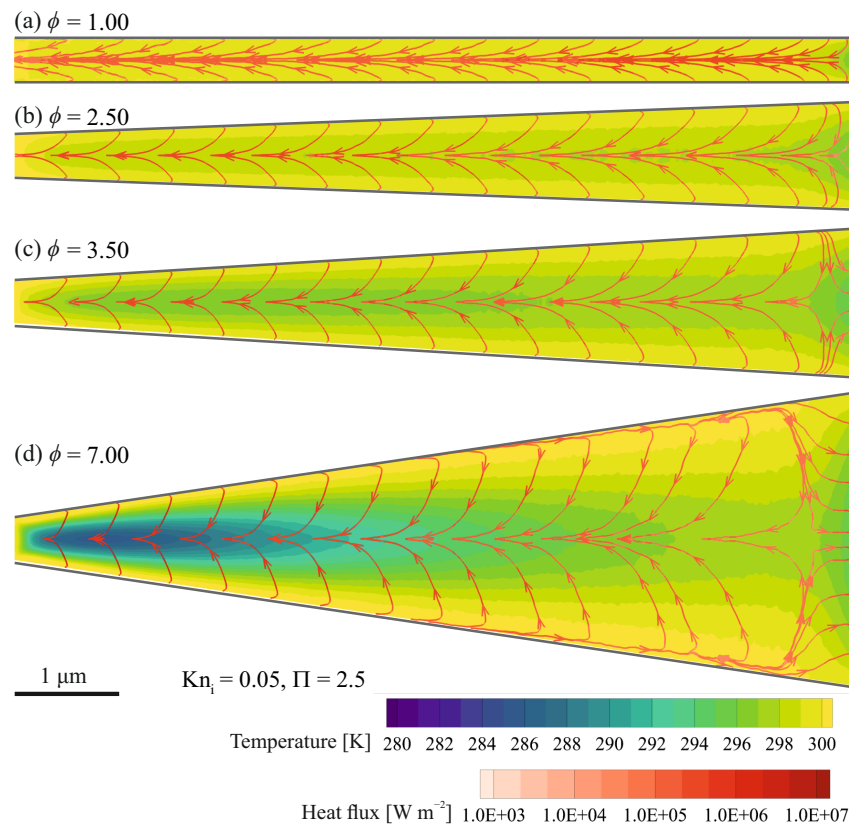


Figure 5. Contours of temperature overlaid with heatlines (coloured by the magnitude of heat flux) obtained from the simulations for microchannels with different divergence angles ϕ . ($\text{Kn}_i = 0.05$ and $\Pi = 2.5$).

Numerical predictions of the gas temperature and Mach number along the channel centreline are presented in Figure 6 for different inlet Knudsen numbers Kn_i at $\phi = 7$ and $\Pi = 2.5$. The bulk gas velocity along the channel and variations in the gas velocity decreases with an increase in the Knudsen number. However, this reduction in the velocity magnitude and its variations becomes insignificant for $\text{Kn}_i \geq 1$. Variation in gas velocity along the channel and the molecular collision frequency decreases with an increase in Knudsen number, limiting the variation in gas temperature along the channel. The magnitude of temperature drop close to the channel outlet also decreases with increasing inlet Knudsen number. Moreover, the predicted gas temperatures close to the channel inlet are slightly higher than the inlet gas temperature T_i because of the augmentation of the temperature jump with increasing Knudsen number [37].

The influence of the Knudsen number on the thermal field and heat flow direction in a divergent channel with $\phi = 7$ and $\Pi = 2.5$ is shown in Figure 7. The temperature gradient in the channel decreases with an increase in Knudsen number, decreasing the contribution of the Fourier heat transfer to the net heat flow. According to Figure 7c,d, at sufficiently large Kn_i , the heat flow in the channel is merely toward the channel inlet, which demonstrates the domination of the pressure gradient in the net heat flow direction, intensifying the counter-gradient cold-to-hot heat transfer (also known as anti-Fourier heat transfer). Moreover, the total heat flow rate decreases with increasing Knudsen number. The distance between the thermal separation point and the channel outlet increases with a decrease in Kn_i .

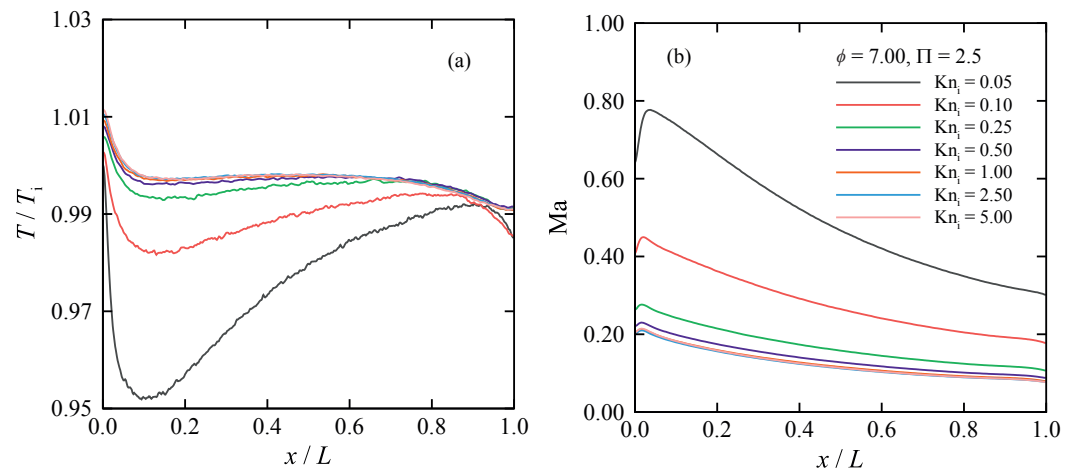


Figure 6. The effect of rarefaction on the profiles of (a) gas temperature and (b) Mach number along the microchannel centreline ($\phi = 7.00$ and $\Pi = 2.5$). The inlet temperature (T_i) is used to non-dimensionalise the predicted temperatures.

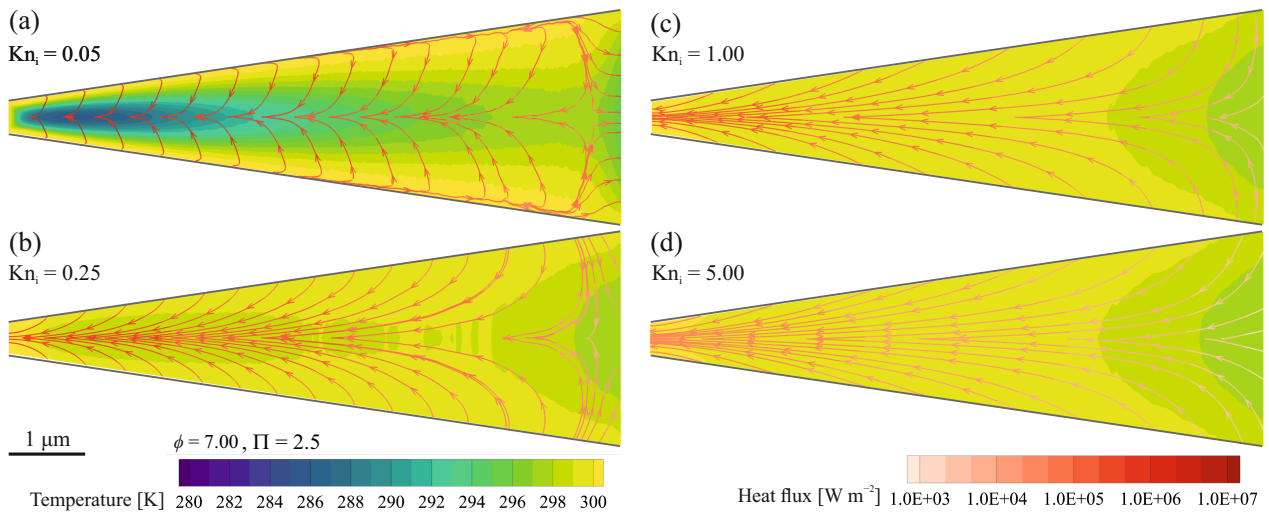


Figure 7. Heatlines (coloured by the magnitude of heat flux) overlaid on contours of dimensionless temperature (T/T_i) predicted for different inlet Knudsen numbers Kn_i . $\phi = 7.00$ and $\Pi = 2.5$.

The bulk gas velocity and temperature in the channel decrease with a decrease in the inlet-to-outlet pressure ratio Π , as shown in Figure 8. Increasing the inlet-to-outlet pressure ratio increases the gas kinetic energy and decreases its internal energy. The thermal field as well as the heat lines are shown in Figure 9 for channels with a divergence angle of $\phi = 7$ and Knudsen number of 0.05. The magnitude of the thermal gradient close to the channel outlet increases with decreasing the pressure ratio Π , which enhances the contribution of the thermal gradient to the net heat flow; this affects the net heat flow direction and leads to the occurrence of thermal separation farther away from the channel outlet. The heat generated in the Knudsen layer due to viscous dissipation diminishes with decreasing inlet-to-outlet pressure ratio Π , decreasing the contribution of thermal gradients to the net heat flow close to the channel walls.

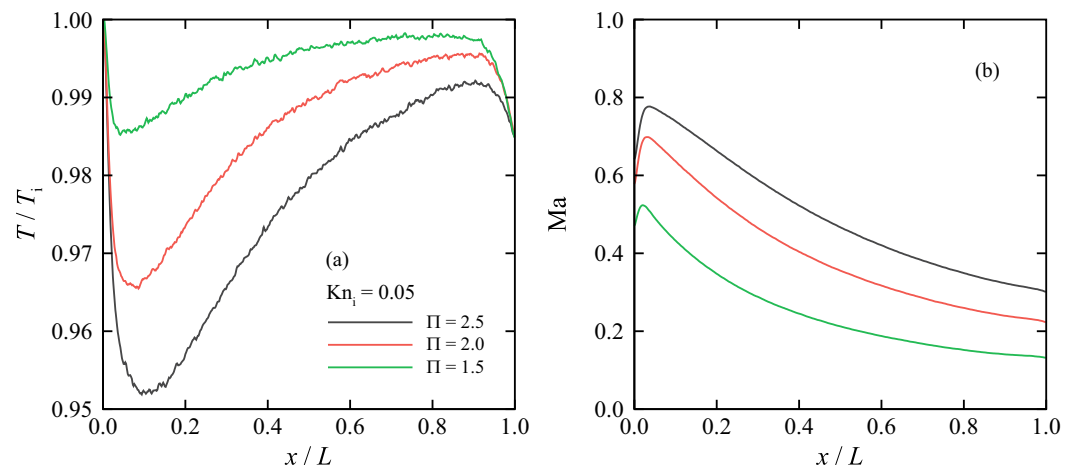


Figure 8. The effect of the inlet-to-outlet pressure ratio Π on the profiles of (a) gas temperature and (b) Mach number along the microchannel centreline ($\phi = 7.00$ and $Kn = 0.05$). The inlet temperature (T_i) is used to non-dimensionalise the predicted temperatures.

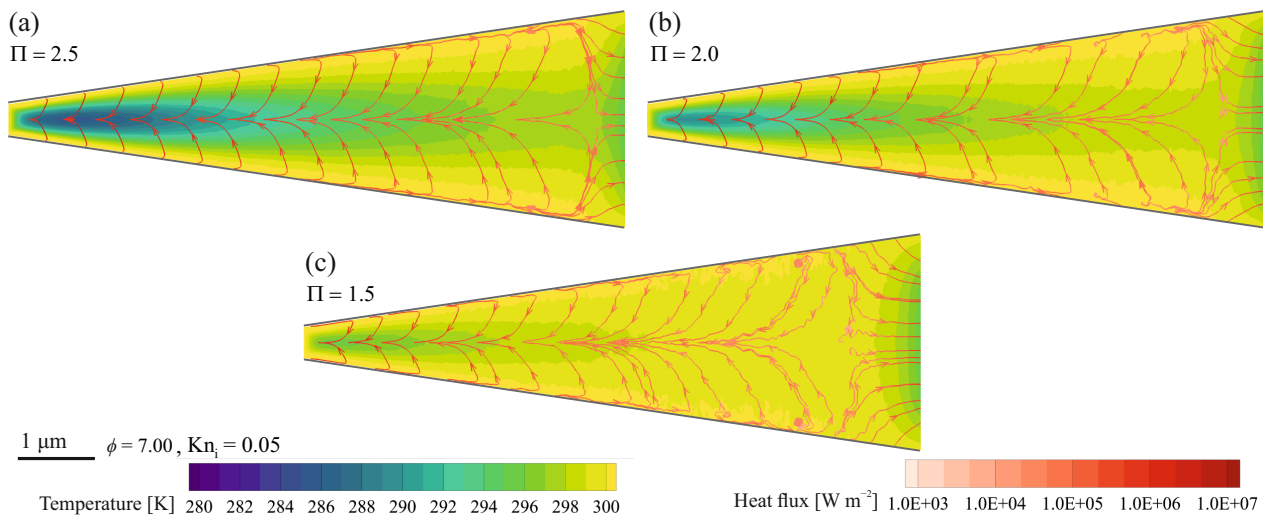


Figure 9. The influence of the inlet-to-outlet pressure ratio Π on the thermal field (contours) and heat flow direction (coloured by the magnitude of heat flux). $Kn_i = 0.05$ and $\phi = 7$.

The influence of the tangential accommodation coefficient (α) on the profiles of temperature and velocity along divergent channels is shown in Figure 10 for $\Pi = 2.5$ and $Kn_i = 0.05$. For all the cases considered in the present work, decreasing the tangential accommodation coefficient weakens the interactions between the gas molecules and the channel walls, leading to an increase in the gas velocity. A similar behaviour has also been observed both experimentally and numerically for rarefied gas flows in microchannels with uniform cross-sections [37,50,51,69]. As expected, the augmentation of gas velocity in the channel results in an increase in the kinetic energy and a decrease in internal energy and thus the gas temperature. The results presented in Figure 11 show that the gas reaches supersonic velocities when $\alpha = 0$ (i.e., specular reflection); this happens for the case with $\phi = 7.0$ only when $\alpha = 0.5$ and does not happen when $\alpha = 1$ (i.e., fully-diffused reflection).

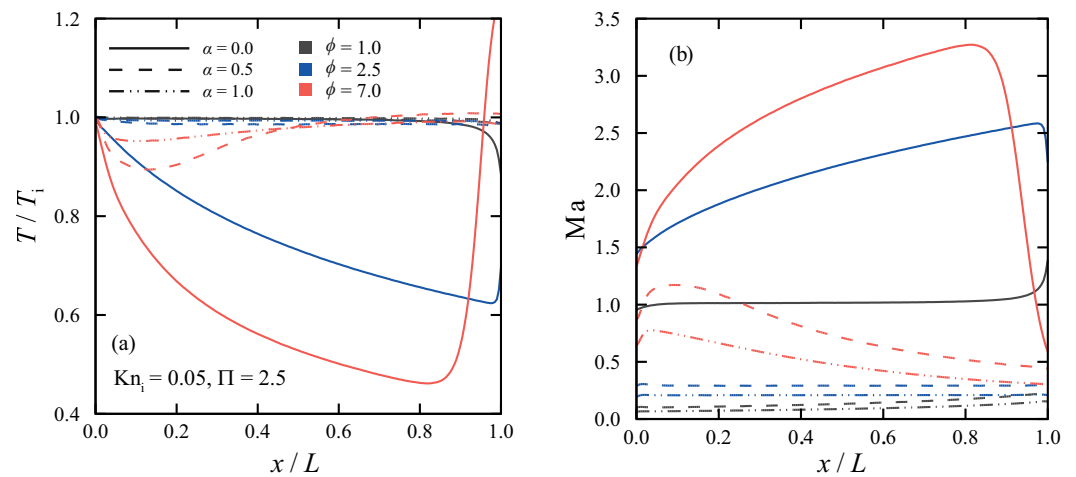


Figure 10. The effect of the tangential accommodation coefficient α on the profiles of (a) gas temperature and (b) Mach number along the microchannel centreline ($\Pi = 2.5$ and $\text{Kn}_i = 0.05$). The inlet temperature (T_i) is used to non-dimensionalise the predicted temperatures.

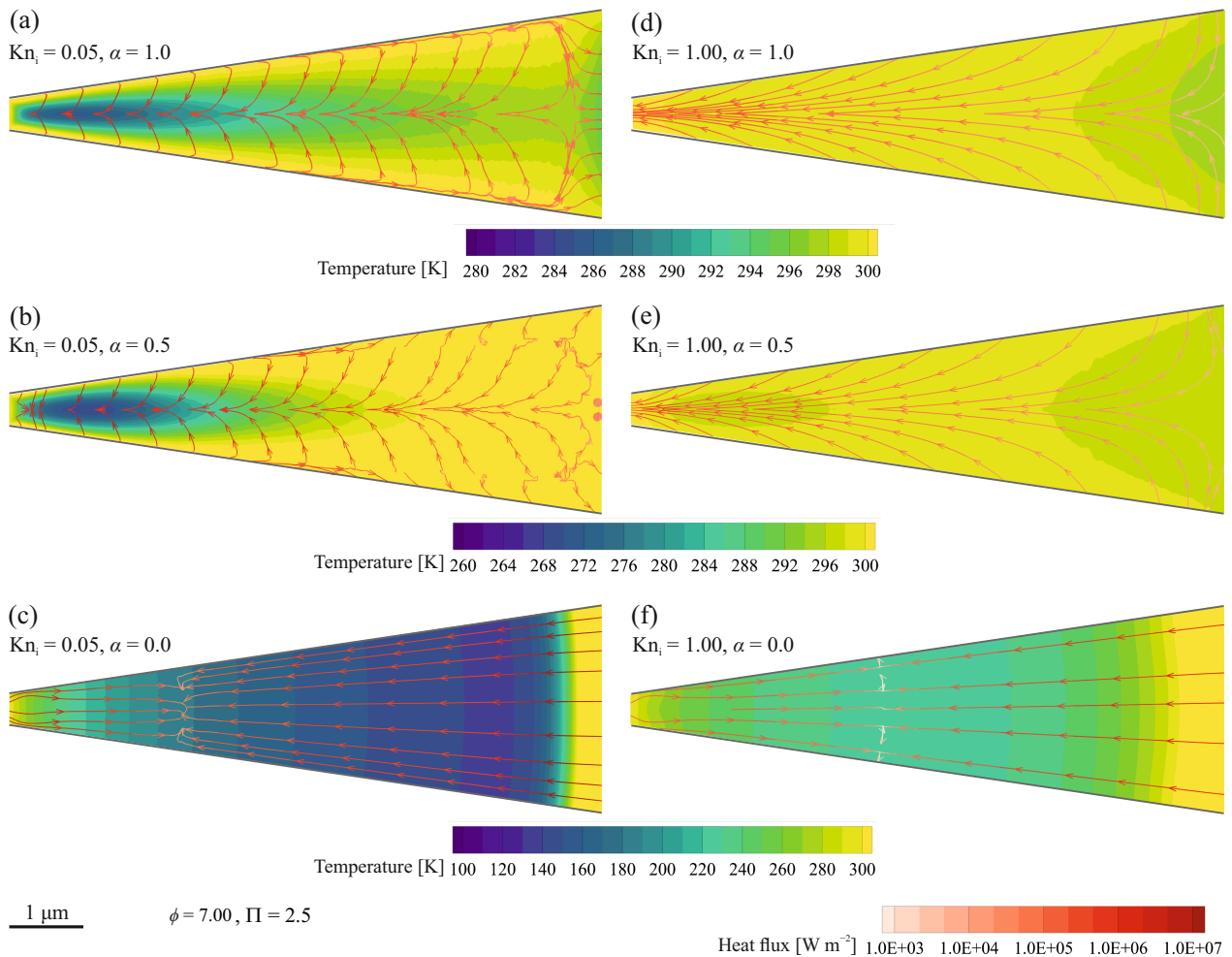


Figure 11. The influence of the tangential accommodation coefficient α on the thermal field (contours) and heat flow direction (coloured by the magnitude of heat flux). $\Pi = 2.5$ and $\phi = 7$.

The results presented in Figure 11 show that heat and fluid flow patterns in the channel are sensitive to the value of the tangential accommodation coefficient α , particularly for low values of the Knudsen number. The number of gas molecules contributing to the adiabatic

exchange of energy increases with decreasing values of the tangential accommodation coefficient α , increasing the contribution of thermal gradients to the net heat flow. Reducing the value of the tangential accommodation coefficient to $\alpha = 0$ as an extreme condition, it is observed that the heat flow converges to a sink point, where pressure gradients balance thermal gradients. Heat lines are directed toward the channel outlet in regions where thermal gradients dominate the net heat flow.

6. Conclusions

Two-dimensional numerical simulations based on the direct simulation Monte Carlo (DSMC) method were performed to predict thermal and flow fields of pressure-driven nitrogen flow in divergent microchannels. A wide range of Knudsen numbers was studied covering the slip to the free molecular rarefaction regimes. Moreover, the influences of microchannel divergence angle, inlet-to-outlet pressure ratio, and incomplete surface accommodation were investigated. The following conclusions were drawn based on the present study.

The influence of thermal gradient on net heat flow direction increases with an increase in the divergence angle of the microchannel and can lead to the occurrence of thermal separation even when hydrodynamic separation is absent. The contribution of the pressure gradient in determining the heat flow direction enhances with an increase in the Knudsen number. At sufficiently large Knudsen numbers, the heat flow is only toward the channel inlet. Cold-to-hot heat transfer (also known as anti-Fourier heat transfer) was observed in the microchannel as a result of nonequilibrium effects. Viscous dissipation in the Knudsen layer diminishes with decreasing applied pressure ratio, which results in the domination of the pressure gradient influence on heat flow close to the channel walls.

Further studies may focus on realising the effects of the molecular weight and structure, or different gas mixtures on thermal and fluid flow fields inside micro- and nanochannels with with complex geometries.

Author Contributions: Conceptualization, A.E. and E.R.; methodology, A.E.; software, A.E. and V.S.; validation, A.E.; formal analysis, A.E.; investigation, A.E.; resources, A.E., V.S. and E.R.; data curation, A.E. and V.S.; writing—original draft preparation, A.E.; writing—review and editing, A.E., V.S. and E.R.; visualization, A.E. and V.S.; supervision, A.E. and E.R.; project administration, A.E. All authors have read and agreed to the published version of the manuscript.

Funding: This research received no external funding. The APC was funded by the Delft University of Technology.

Data Availability Statement: The data presented in this study are available on request from the corresponding author.

Conflicts of Interest: The authors declare no conflict of interest.

Abbreviations

The following abbreviations are used in this manuscript:

DSMC	Direct simulation Monte Carlo
NTC	No time counter
TAS	Transient adaptive sub-celling
VHS	Variable hard sphere
PPC	Particle per cell
NSF	Navier–Stokes–Fourier
MEMS	Micro-electromechanical systems
OpenFOAM	Open Source Field Operation and Manipulation

References

1. Würger, A. Leidenfrost Gas Ratchets Driven by Thermal Creep. *Phys. Rev. Lett.* **2011**, *107*. [[CrossRef](#)]
2. Gebhard, U.; Hein, H.; Schmidt, U. Numerical investigation of fluidic micro-oscillators. *J. Micromech. Microeng.* **1996**, *6*, 115–117. [[CrossRef](#)]
3. Jiang, X.; Zhou, Z.; Huang, X.; Li, Y.; Yang, Y.; Liu, C. Micronozzle/diffuser flow and its application in micro valveless pumps. *Sens. Actuators A Phys.* **1998**, *70*, 81–87. [[CrossRef](#)]
4. Duryodhan, V.S.; Singh, A.; Singh, S.G.; Agrawal, A. A simple and novel way of maintaining constant wall temperature in microdevices. *Sci. Rep.* **2016**, *6*. [[CrossRef](#)]
5. Yang, M.; Ripoll, M. Thermoosmotic microfluidics. *Soft Matter* **2016**, *12*, 8564–8573. [[CrossRef](#)] [[PubMed](#)]
6. Bordbar, A.; Kheirandish, S.; Taassob, A.; Kamali, R.; Ebrahimi, A. High-viscosity liquid mixing in a slug-flow micromixer: A numerical study. *J. Flow Chem.* **2020**, *10*, 449–459. [[CrossRef](#)]
7. Agrawal, A. A Comprehensive Review on Gas Flow in Microchannels. *Int. J. Micro Nano Scale Transp.* **2011**, *2*, 1–40. [[CrossRef](#)]
8. Ebrahimi, A.; Roohi, E.; Kheradmand, S. Numerical study of liquid flow and heat transfer in rectangular microchannel with longitudinal vortex generators. *Appl. Therm. Eng.* **2015**, *78*, 576–583. [[CrossRef](#)]
9. Ebrahimi, A.; Rikhtegar, F.; Sabaghan, A.; Roohi, E. Heat transfer and entropy generation in a microchannel with longitudinal vortex generators using nanofluids. *Energy* **2016**, *101*, 190–201. [[CrossRef](#)]
10. Ferziger, J.H.; Kaper, H.G.; Gross, E.P. Mathematical Theory of Transport Processes in Gases. *Am. J. Phys.* **1973**, *41*, 601–603. [[CrossRef](#)]
11. Johnson, R.W. *Handbook of Fluid Dynamics*; CRC Press: Boca Raton, FL, USA, 2016.
12. Gad-el-Hak, M. *The MEMS Handbook*; CRC Press: Boca Raton, FL, USA, 2005.
13. Kirby, B.J. *Micro- and Nanoscale Fluid Mechanics*; Cambridge University Press: Leiden, The Netherlands, 2010.
14. Roy, S.; Raju, R.; Chuang, H.F.; Cruden, B.A.; Meyyappan, M. Modeling gas flow through microchannels and nanopores. *J. Appl. Phys.* **2003**, *93*, 4870–4879. [[CrossRef](#)]
15. Karniadakis, G.E.; Beskok, A.; Aluru, N. *Microflows and Nanoflows*; Springer: New York, NY, USA, 2005. [[CrossRef](#)]
16. Shen, C. *Rarefied Gas Dynamics*; Springer: Berlin/Heidelberg, Germany, 2005. [[CrossRef](#)]
17. Kara, V.; Yakhot, V.; Ekinci, K. Generalized Knudsen Number for Unsteady Fluid Flow. *Phys. Rev. Lett.* **2017**, *118*. [[CrossRef](#)]
18. Bird, G.A. *Molecular Gas Dynamics and the Direct Simulation of Gas Flows*; Clarendon Press: Oxford, UK, 1994.
19. Jakobsen, H.A. *Chemical Reactor Modeling*; Springer: Berlin/Heidelberg, Germany, 2008. [[CrossRef](#)]
20. Zheng, Y.; Garcia, A.L.; Alder, B.J. Comparison of Kinetic Theory and Hydrodynamics for Poiseuille Flow. *J. Stat. Phys.* **2002**, *109*, 495–505. [[CrossRef](#)]
21. Arkilic, E.B.; Breuer, K.S.; Schmidt, M.A. Mass flow and tangential momentum accommodation in silicon micromachined channels. *J. Fluid Mech.* **2001**, *437*, 29–43. [[CrossRef](#)]
22. Arlemark, E.J.; Dadzie, S.K.; Reese, J.M. An Extension to the Navier-Stokes-Fourier Equations by Considering Molecular Collisions With Boundaries. In Proceedings of the ASME 2008 6th International Conference on Nanochannels, Microchannels, and Minichannels, Darmstadt, Germany, 23–25 June 2008; ASME: New York, NY, USA, 2008. [[CrossRef](#)]
23. Zade, A.Q.; Ahmadzadegan, A.; Renksizbulut, M. A detailed comparison between Navier–Stokes and DSMC simulations of multicomponent gaseous flow in microchannels. *Int. J. Heat Mass Transf.* **2012**, *55*, 4673–4681. [[CrossRef](#)]
24. Torrilhon, M.; Struchtrup, H. Modeling Micro Mass and Heat Transfer for Gases Using Extended Continuum Equations. *J. Heat Transf.* **2009**, *131*, 033103. [[CrossRef](#)]
25. Varoutis, S.; Day, C.; Sharipov, F. Rarefied gas flow through channels of finite length at various pressure ratios. *Vacuum* **2012**, *86*, 1952–1959. [[CrossRef](#)]
26. Kandlikar, S.G.; Colin, S.; Peles, Y.; Garimella, S.; Pease, R.F.; Brandner, J.J.; Tuckerman, D.B. Heat Transfer in Microchannels—2012 Status and Research Needs. *J. Heat Transf.* **2013**, *135*, 091001. [[CrossRef](#)]
27. Fang, Y.; Liou, W.W. Computations of the Flow and Heat Transfer in Microdevices Using DSMC With Implicit Boundary Conditions. *J. Heat Transf.* **2002**, *124*, 338. [[CrossRef](#)]
28. Liou, W.; Fang, Y. Heat transfer in microchannel devices using DSMC. *J. Microelectromech. Syst.* **2001**, *10*, 274–279. [[CrossRef](#)]
29. Zhang, M.; Day, C.; Varoutis, S.; Cai, G. Rarefied gas flow into vacuum through short tubes at variable wall temperatures. *J. Vac. Sci. Technol. A Vacuum Surfaces Film* **2017**, *35*, 021604. [[CrossRef](#)]
30. Hemadri, V.; Duryodhan, V.S.; Agrawal, A. Liquid and gas flows in microchannels of varying cross section: A comparative analysis of the flow dynamics and design perspectives. *Microfluid. Nanofluid.* **2018**, *22*. [[CrossRef](#)]
31. Varade, V.; Duryodhan, V.; Agrawal, A.; Pradeep, A.; Ebrahimi, A.; Roohi, E. Low Mach number slip flow through diverging microchannel. *Comput. Fluids* **2015**, *111*, 46–61. [[CrossRef](#)]
32. Varade, V.; Agrawal, A.; Pradeep, A.M. Slip flow through a converging microchannel: experiments and 3D simulations. *J. Micromech. Microeng.* **2015**, *25*, 025015. [[CrossRef](#)]
33. Hemadri, V.; Varade, V.V.; Agrawal, A.; Bhandarkar, U.V. Investigation of rarefied gas flow in microchannels of non-uniform cross section. *Phys. Fluids* **2016**, *28*, 022007. [[CrossRef](#)]
34. Hemadri, V.; Varade, V.V.; Agrawal, A.; Bhandarkar, U.V. Rarefied gas flow in converging microchannel in slip and early transition regimes. *Phys. Fluids* **2017**, *29*, 032002. [[CrossRef](#)]

35. Milićev, S.S.; Stevanović, N.D. Gas Flow in Microchannels and Nanochannels With Variable Cross Section for All Knudsen and All Mach Number Values. *J. Fluids Eng.* **2020**, *143*. [[CrossRef](#)]
36. Ohwada, T.; Sone, Y.; Aoki, K. Numerical analysis of the Poiseuille and thermal transpiration flows between two parallel plates on the basis of the Boltzmann equation for hard-sphere molecules. *Phys. Fluids A Fluid Dyn.* **1989**, *1*, 2042–2049. [[CrossRef](#)]
37. John, B.; Gu, X.J.; Emerson, D.R. Nonequilibrium gaseous heat transfer in pressure-driven plane Poiseuille flow. *Phys. Rev. E* **2013**, *88*. [[CrossRef](#)]
38. Ebrahimi, A.; Roohi, E. Flow and Thermal Fields Investigation in Divergent Micro/Nano Channels. *J. Therm. Eng.* **2016**, *2*, 709–714. [[CrossRef](#)]
39. Ebrahimi, A.; Roohi, E. DSMC investigation of rarefied gas flow through diverging micro- and nanochannels. *Microfluid. Nanofluid.* **2017**, *21*. [[CrossRef](#)]
40. Guerrieri, D.C.; Cervone, A.; Gill, E. Analysis of Nonisothermal Rarefied Gas Flow in Diverging Microchannels for Low-Pressure Microresistojets. *J. Heat Transf.* **2016**, *138*, 112403. [[CrossRef](#)]
41. Kannan, A.S.; Narahari, T.S.B.; Bharadhwaj, Y.; Mark, A.; Sardina, G.; Maggiolo, D.; Sasic, S.; Ström, H. The Knudsen Paradox in Micro-Channel Poiseuille Flows with a Symmetric Particle. *Appl. Sci.* **2020**, *11*, 351. [[CrossRef](#)]
42. Taassob, A.; Kamali, R.; Bordbar, A. Investigation of rarefied gas flow through bended microchannels. *Vacuum* **2018**, *151*, 197–204. [[CrossRef](#)]
43. Shah, N.; Agrawal, A.; Bhandarkar, U. 3D study of temperature drop behavior of subsonic rarefied gas flow in microchannel. *Numer. Heat Transf. Part A Appl.* **2018**, *73*, 654–665. [[CrossRef](#)]
44. Balaj, M.; Roohi, E.; Mohammadzadeh, A. Regulation of anti-Fourier heat transfer for non-equilibrium gas flows through micro/nanochannels. *Int. J. Therm. Sci.* **2017**, *118*, 24–39. [[CrossRef](#)]
45. Gavasane, A.; Agrawal, A.; Pradeep, A.M.; Bhandarkar, U. Simulation of a temperature drop for the flow of rarefied gases in microchannels. *Numer. Heat Transf. Part A Appl.* **2017**, *71*, 1066–1079. [[CrossRef](#)]
46. Hong, C.; Yamamoto, T.; Asako, Y.; Suzuki, K. Heat Transfer Characteristics of Compressible Laminar Flow Through Microtubes. *J. Heat Transf.* **2012**, *134*, 011602. [[CrossRef](#)]
47. Roohi, E.; Darbandi, M.; Mirjalili, V. Direct Simulation Monte Carlo Solution of Subsonic Flow Through Micro/Nanoscale Channels. *J. Heat Transf.* **2009**, *131*, 092402. [[CrossRef](#)]
48. Hong, C.; Asako, Y. Heat Transfer Characteristics of Gaseous Flows in a Microchannel and a Microtube with Constant Wall Temperature. *Numer. Heat Transf. Part A Appl.* **2007**, *52*, 219–238. [[CrossRef](#)]
49. Zhen, C.E.; Hong, Z.C.; Lin, Y.J.; Hong, N.T. Comparison of 3-D and 2-D DSMC Heat Transfer Calculations of Low-Speed Short Microchannel Flows. *Numer. Heat Transf. Part A Appl.* **2007**, *52*, 239–250. [[CrossRef](#)]
50. Acharya, T.; Falgout, J.; Schoegl, I.; Martin, M.J. Measurement of Variation of Momentum Accommodation Coefficients with Molecular Mass and Structure. *J. Thermophys. Heat Transf.* **2019**, *33*, 773–778. [[CrossRef](#)]
51. Graur, I.A.; Perrier, P.; Ghozlani, W.; Méolans, J.G. Measurements of tangential momentum accommodation coefficient for various gases in plane microchannel. *Phys. Fluids* **2009**, *21*, 102004. [[CrossRef](#)]
52. White, C.; Borg, M.; Scanlon, T.; Longshaw, S.; John, B.; Emerson, D.; Reese, J. dsmcFoam+: An OpenFOAM based direct simulation Monte Carlo solver. *Comput. Phys. Commun.* **2018**, *224*, 22–43. [[CrossRef](#)]
53. Scanlon, T.J.; White, C.; Borg, M.K.; Palharini, R.C.; Farbar, E.; Boyd, I.D.; Reese, J.M.; Brown, R.E. Open-Source Direct Simulation Monte Carlo Chemistry Modeling for Hypersonic Flows. *AIAA J.* **2015**, *53*, 1670–1680. [[CrossRef](#)]
54. Palharini, R.C.; White, C.; Scanlon, T.J.; Brown, R.E.; Borg, M.K.; Reese, J.M. Benchmark numerical simulations of rarefied non-reacting gas flows using an open-source DSMC code. *Comput. Fluids* **2015**, *120*, 140–157. [[CrossRef](#)]
55. Su, C.; Tseng, K.; Cave, H.; Wu, J.; Lian, Y.; Kuo, T.; Jermy, M. Implementation of a transient adaptive sub-cell module for the parallel-DSMC code using unstructured grids. *Comput. Fluids* **2010**, *39*, 1136–1145. [[CrossRef](#)]
56. Oran, E.; Oh, C.; Cybyk, B. DIRECT SIMULATION MONTE CARLO: Recent Advances and Applications. *Annu. Rev. Fluid Mech.* **1998**, *30*, 403–441. [[CrossRef](#)]
57. Alexander, F.J.; Garcia, A.L.; Alder, B.J. Cell size dependence of transport coefficients in stochastic particle algorithms. *Phys. Fluids* **1998**, *10*, 1540–1542. [[CrossRef](#)]
58. Cai, C.; Boyd, I.D.; Fan, J.; Candler, G.V. Direct Simulation Methods for Low-Speed Microchannel Flows. *J. Thermophys. Heat Transf.* **2000**, *14*, 368–378. [[CrossRef](#)]
59. Shen, C.; Fan, J.; Xie, C. Statistical simulation of rarefied gas flows in micro-channels. *J. Comput. Phys.* **2003**, *189*, 512–526. [[CrossRef](#)]
60. Sun, Z.X.; Tang, Z.; He, Y.L.; Tao, W.Q. Proper cell dimension and number of particles per cell for DSMC. *Comput. Fluids* **2011**, *50*, 1–9. [[CrossRef](#)]
61. Shu, C.; Mao, X.; Chew, Y. Particle number per cell and scaling factor effect on accuracy of DSMC simulation of micro flows. *Int. J. Numer. Methods Heat Fluid Flow* **2005**, *15*, 827–841. [[CrossRef](#)]
62. Radtke, G.A.; Hadjiconstantinou, N.G.; Wagner, W. Low-noise Monte Carlo simulation of the variable hard sphere gas. *Phys. Fluids* **2011**, *23*, 030606. [[CrossRef](#)]
63. Hadjiconstantinou, N.G.; Garcia, A.L.; Bazant, M.Z.; He, G. Statistical error in particle simulations of hydrodynamic phenomena. *J. Comput. Phys.* **2003**, *187*, 274–297. [[CrossRef](#)]

64. White, C.; Borg, M.K.; Scanlon, T.J.; Reese, J.M. A DSMC investigation of gas flows in micro-channels with bends. *Comput. Fluids* **2013**, *71*, 261–271. [[CrossRef](#)]
65. Hadjiconstantinou, N.G.; Simek, O. Constant-Wall-Temperature Nusselt Number in Micro and Nano-Channels. *J. Heat Transf.* **2001**, *124*, 356–364. [[CrossRef](#)]
66. Sone, Y. (Ed.) *Molecular Gas Dynamics*; Birkhäuser: Boston, MA, USA, 2007. [[CrossRef](#)]
67. Gu, X.; Barber, R.; Emerson, D. How Far Can 13 Moments Go in Modeling Microscale Gas Phenomena? *Nanoscale Microscale Thermophys. Eng.* **2007**, *11*, 85–97. [[CrossRef](#)]
68. Mahdavi, A.M.; Roohi, E. Investigation of cold-to-hot transfer and thermal separation zone through nano step geometries. *Phys. Fluids* **2015**, *27*, 072002. [[CrossRef](#)]
69. Cercignani, C.; Lampis, M.; Lorenzani, S. Variational approach to gas flows in microchannels. *Phys. Fluids* **2004**, *16*, 3426–3437. [[CrossRef](#)]